Applied Catalysis B: Environmental 249 (2019) 147–154

Contents lists available at ScienceDirect

Applied Catalysis B: Environmental

journal homepage: www.elsevier.com/locate/apcatb

Bottom-up MOF-intermediated synthesis of 3D hierarchical flower-like cobalt-based homobimetallic phophide composed of ultrathin nanosheets for highly efficient oxygen evolution reaction

Guoliang Li[a], Xiaobing Zhang[b], He Zhang[a], Chunyang Liao[a,*], Guibin Jiang[a]

[a] State Key Laboratory for Environmental Chemistry and Eco-toxicology, Research Center for Eco-Environmental Sciences, Chinese Academy of Sciences, Beijing 100085, China

[b] Key Laboratory of Microbial Technology for Industrial Pollution Control of Zhejiang Province, College of Environment, Zhejiang University of Technology, Hangzhou 310014, China

ARTICLE INFO

Keywords:
Synthesis
Hierarchical superstructure
Ultrathin nanosheet
Phosphide
Oxygen evolution reaction

ABSTRACT

In demand of implementing the replacement of fossil fuels, efficient oxygen evolution reaction (OER) catalysts are required in producing clean and low-cost hydrogen fuels *via* water splitting, the urgency and great necessity of which make it one of the greatest challenges for scientists and engineers concerned with research on energy issues. A novel bottom-up one-pot solvothermal strategy followed by low-temperature phosphorization was developed to prepare 3D hierarchical flower-like materials composed of ultrathin cobalt based bimetallic phosphide nanosheets (CoM-P-3DHFLMs) as cost-effective OER electrocatalysts, which are highly efficient and durable. Due to their unique structural and compositional advantages, the CoM-P-3DHFLMs not only achieve satisfying electrocatalytic efficiencies (η@10 mA cm^{-2} = 292 mV, 318 mV, and 307 mV for CoNi-, CoMn-, and CoCu-P-3DHFLM, respectively) comparable to IrO_2 and RuO_2 counterparts, but also exhibit long-term stability with subtle decrement after 10 h. The advantages of high efficiency, good stability, and free of noble metal make the as-prepared 3DHFLMs promising candidates for OER.

1. Introduction

For the past few decades, in order to meet the rising demand for functional materials of high application performance, structure-directing strategy has been an enduring hotspot in material chemistry to synthesize materials with diverse morphologies, e.g. 1D nanoparticles, 2D nanosheets, and 3D complicated structures, among which 3D hierarchical structures composed of 1D nanoparticles (e.g. porous spheres, hollow spheres and multi-shelled spheres) or 2D nanosheets (hierarchical tubes, boxes, and bionic structures) have shown outstanding advantages due to their harmonized merits of both the composed subunits of lower dimensions and the subsequent unique 3D hierarchical structure [1–6]. Distinct from the bulk materials, those ultrathin 2D graphene-like nanosheets based materials, which feature a small thickness of a few nanometers and a large micrometer scale lateral size, exhibit unique physical and chemical characteristics due to the very large surface-to-volume ratio and the quantum-confinement effect [7–9]. In particular, 2D nanosheets based materials hold great promise as electrode materials for electrochemical energy conversion and storage [10–13].

Intensive studies have shown that the P element is promising in constructing effective catalysts either as dopant [14,15] or as phosphide [16,17] due to that the electronegativity of P atoms tends to grasp the electrons from metal atoms [18,19]. Most recently, the metal phosphides have been reported to be active and robust in electrocatalysis [20–24], lithium-ion and sodium-ion batteries [25,26]. Especially, nanostructured transition metal phosphides (Ni_2P, CoP, FeP) have been considered as a class of effective catalysts for HER and/or OER. P is deemed to function for the promising activity of phosphides, which possess lone-pair electrons in 3p orbitals and vacant 3d orbitals, and thus can induce local charge density and accommodate the surface charge state [27]. Generally, synthesis of phosphide can be realized by phosphidation of corresponding oxides [28,29] or hydroxide [16,30]. Moreover, MOMs (Metal-Organic Materials), an emerging class of porous materials consisting of metal-organic frameworks (MOFs) and metal-organic polyhedra (MOPs), which are assembled by metal centers and organic ligands, have become an intriguing phosphidation target for realizing a better electrocatalytic performance due to their unique

* Corresponding author.
E-mail address: cyliao@rcees.ac.cn (C. Liao).

https://doi.org/10.1016/j.apcatb.2019.03.007
Received 26 December 2018; Received in revised form 23 February 2019; Accepted 1 March 2019
Available online 02 March 2019
0926-3373/

and beneficial characteristics [23,31–37].

The outstanding features of MOMs involve high specific surface area, abundant pore system, and richness in organic ligands, which indeed favor many application fields [31,38]. Up to the date, two main ways, the direct in-situ way and the indirect post-synthetic process, are adopted to shape the MOMs. These methods normally result in either MOM crystalline powders with different sizes or solid topologies (e.g. nanoparticles and polyhedra), or secondary construction based on preformed crystalline powders (e.g. thin films or aggregated spherical particles). However, the bulk existence confines their efficiency in structure-oriented application fields. Therefore, rational tailoring of their shapes, sizes, and pore structures, which are crucial for application, have been paid great attention [17,38–41]. Though certain progress has been made, exquisite design and synthesis of purpose-targeting nanostructures remain a great challenge. More complicated constructions such as the abovementioned 3D hierarchical superstructures constructed by 2D subunits with the unique derivative properties are rarely reported.

Inspired by those findings, we demonstrate here a rational bottom-up synthesis method to fabricate a three-dimensional hierarchical flower-like MOM (3DHFLM), which simultaneously realizes both the merits of MOM and the structure privilege of 2D nanosheets and the derived 3D hierarchical structure. The synthesis procedure is schematically illustrated in Fig. 1. The novel MOM is fabricated by a solvothermal process using 2-methylimidazole (2-MeIm) and cobalt ions as ingredients and methanol as solution. Although the reagents are similar to those of used to synthesize the polyhedral ZIF-67, the architecture of the as-prepared sample is thoroughly different from the solid polyhedral trunk of the ZIF-67, exhibiting a unique 3D hierarchical structure composed of 2D ultrathin nanosheets. Also, this strategy is distinct to the traditional top-down method for preparing MOM with complicated structures that must pre-synthesize a maternal template, only a one-pot process is needed to fulfill the synthesis procedure. Finally, the as-prepared 3DHFLMs are converted to phosphide composites by treatment with NaH_2PO_2 at 300 °C for 2 h in a nitrogen atmosphere. Impressively, due to the strong coordination of imidazole with other metal ions (Ni, Cu, Mn) similar to Co in respect of the ionic radium in crystals and electronegativity, a series of Co based homogeneous bimetallic 3DHFLMs can be also successfully fabricated with the same synthesis protocol. To the best of our knowledge, this is the first example of the construction of 3D hierarchical MOMs by a simple bottom-up strategy. Furthermore, it is not out of expectation that the as-prepared phosphorized homobimetallic 3DHFLMs show highly efficient activity toward OER.

2. Results and discussions

The morphology of the precursor Co-3DHFLM was characterized by a field-emission scanning electron microscopy (FESEM) and a transmission electron microscopy (TEM). Typical FESEM images (Fig. 2a) indicate that the sample consists of discrete and uniform peony-like microflowers with a size of around 3 μm. The detailed FESEM image of a single microflower (Fig. 2a2) further demonstrates it is composed of randomly-oriented nanosheets forming a three-dimensional hierarchical superstructure. From the enlarged image of a part of a single flower (Fig. 2a3), it can be clearly observed that the nanosheets are extremely thin. Specifically, the SEM images under high voltage scanning (Fig. 2b) give a more exquisite demonstration of the characteristics of good uniformity, complex hierarchy, and ultrathin nanosheet subunits. The TEM images shown in Fig. 2c further verify the 3D hierarchical flower-like superstructure of the sample. The loosely assembled nanosheets are directly shown by the distinct contrast between the curled edges/stacked part and the large continuous nanosheets. The composing nanosheet can be defined as ultrathin with the thickness of approximate 1.5 nm according to atomic force microscopic (AFM) observation (Fig. 2d). Such a one-pot bottom-up synthesis of a MOM with the unique hierarchical architecture featuring the ultrathin primary building subunits and the well-defined secondary 3D hierarchical morphology is very unusual and rarely reported. What is more interesting is that addition of other metal ions, such as Ni, Cu and Mn, can result in bimetallic 3DHFLMs (CoM(Ni, Mn, Cu)-3DHFLMs) without any change in overall morphology, which can be confirmed by the SEM and TEM images (Figs. S1-S3, SI). The energy-dispersive X-ray (EDX) analysis (Figs. S1d-S3d, SI) confirms the precursor CoM-3DHFLMs are composed of Co, M, C, O and N elements, demonstrating the successful integration of the added metal ions without damaging the unique 3D hierarchical structure.

To better understand the intrinsic nature of the as-prepared 3DHFLMs, more characterization techniques were carried out. The X-ray diffraction profile of the Co-3DHFLM (Fig. 2e) exhibits 5 distinct diffraction peaks at 10.76°, 21.83°, 34.00°, 37.95°, and 59.90°, which seems like the pattern of the α-$Co(OH)_2$ (JCPDS: 46-0605), but unfortunately it is not. This prevents us from determining the detailed structural information. However, the obtained XRD can still supply important information to deduce the structure. The asymmetric diffraction peak at 2θ of 34° is termed as “two-dimensional”, since it arises only from layers of the structure normal to the *c* axis [42]. This indicates the obtained sample appears in a hydrotalcite-like α type phase which can be indexed on a triple-layered hexagonal cell [43]. The Co based bimetallic 3DHFLMs (CoM-3DHFLMs) appear in the same XRD patterns to that of Co-3DHFLM without any other new peaks, indicating incorporation of those metal ions does not change the crystal structure of the samples, those metal ions homogeneously intercalate into crystal lattice of Co-3DHFLM. To further determine the composition of the Co-3DHFLM, Fourier transform infrared spectra (FTIR) was investigated. As shown in Fig. S4, the broad peak in the range of 450-770 cm^{-1} can be assigned to δ(OH) and $\tilde{\nu}$(Co−OH) vibrations [44]. The peaks around 1055 and 1632 cm^{-1} are stretching vibrations of Co−OH and δ(H−O−H) respectively, substantiating the above-made assignment of the structure according to the XRD results [45–47]. What is worth noting is that the peak locating at 1349 cm^{-1} represents the characteristic absorption peak of $-CH_3/-CH_2$-. Also, characteristic bands at

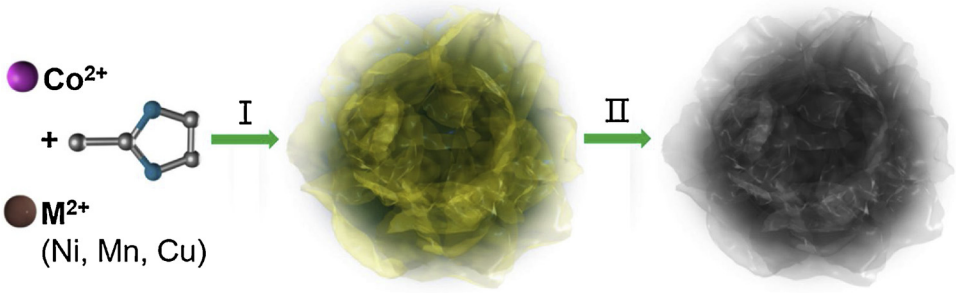

Fig. 1. Schematic illustration of the formation process of CoM-P-3DHFLMs: I) solvothermal reaction of Co^{2+} with 2-methylimidazol to form CoM-3DHFLMs and II) phosphorization of CoM-3DHFLMs to obtain CoM-P-3DHFLMs.

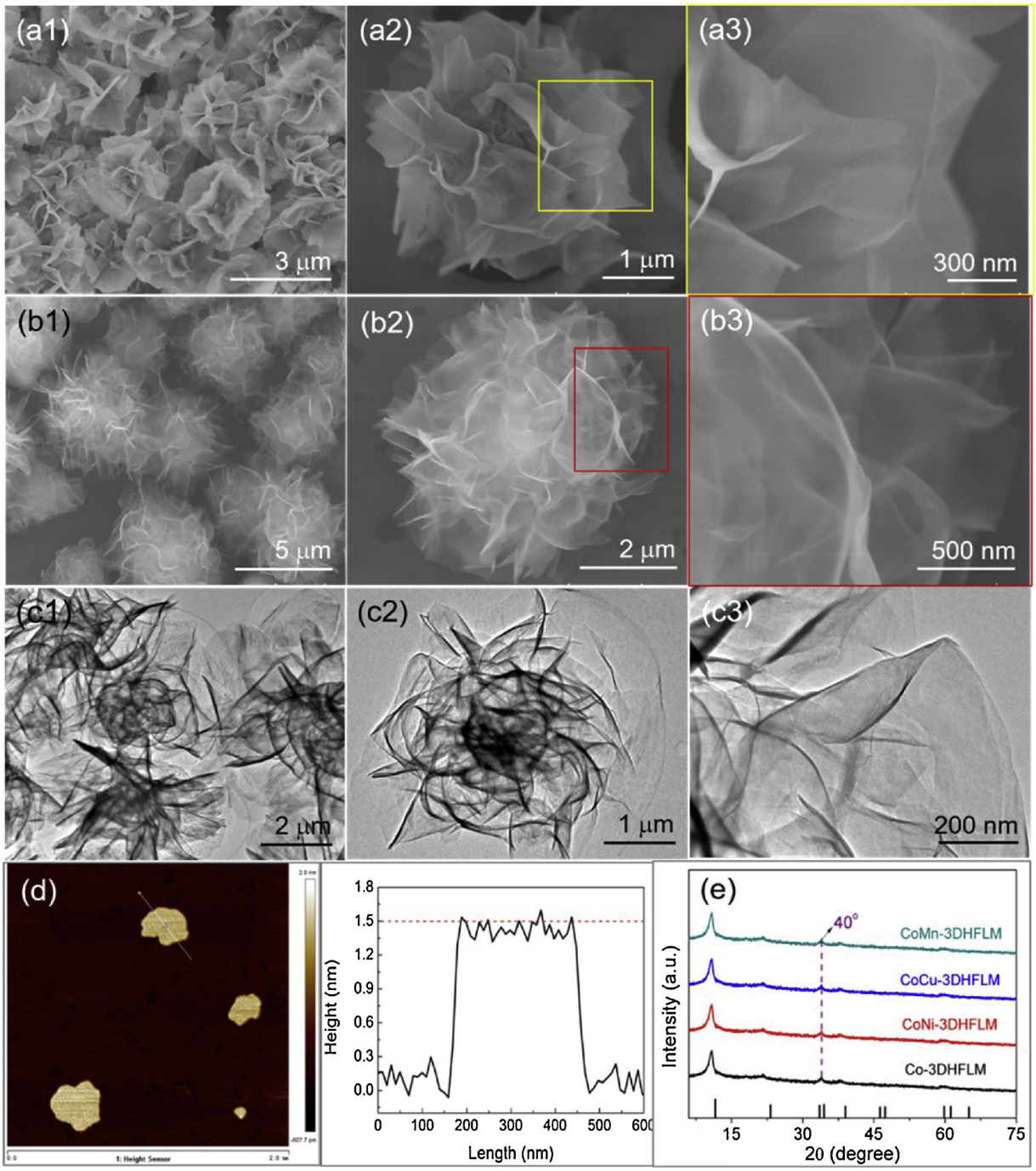

Fig. 2. SEM (a), high voltage SEM (b), TEM (c), AFM (d) of the as-prepared Co-3DHFLM, and XRD patterns of the as-prepared 3DHFLMs (e) compared with the standard JCPDS card (46-0605) of the α-$Co(OH)_2$.

2294 and 2856 cm^{-1} are correlating with stretching vibration of C—H bands of aliphatic groups. To penetrate deeper into the chemical composition, X-ray photoelectronic spectroscopy (XPS) was also performed. The survey spectra (Fig. S5, SI) show that the prepared 3DHFLM contains Co, N, C and O elements. The high-resolution C 1 s spectrum can be deconvolved into four peaks: the sp^2 bonded carbon at 284.8 eV (C—C/C = C), carbon atoms of C-N^+ (285.8 eV), the epoxy at 286.4 eV (C—OH/C—OCo), and the carbonyls at 288.5 eV (O—C═O), indicating the nitrogen bonded carbon, hydroxyl groups and oxygen containing organic functional groups [48,49]. Based on the above information, we reasonably propose that the as-prepared 3DHFLM is a hydrotalcite-like α-type cobalt based complex material containing hydroxyl and oxygen containing organic functional groups. Furthermore, thermogravimetric analysis (TGA) performed from 30 to 900 °C (Fig. S6, SI) shows that the prepared 3DHFLM undergoes a three-step weight loss compared to the one step loss of the ZIF-67, demonstrating the 3DHFLM possesses a much more complicated composition than ZIF-67 particles. The first weight step loss of the 3DHFLM at 197 °C is due to the dehydration of the inserted water molecules and the decomposition of the hydroxide composition. The second and the third weight step loss come from the decomposition of C and N species, respectively, and the net weight loss of the last two steps (7.31% and 2.94%) is consistent with EDX result (7.11% and 3.08%) (Table S1, SI).

To probe the formation mechanism of this unique structure, more experiments were carried out. As we know, the reagents (2-MeIm, Cobalt nitrate and methanol) involved in this work are the same to ZIF-

67, a famous MOF material. Under the same experimental condition of the Co-3DHFLM, when the molar ratio of Co/MeIm decreases to 1/4 (Comparison experiment 1), the typical ZIF-67 particles with uniform shape of rhombic dodecahedron and smooth surface are obtained (Fig. S7a, SI). The XRD pattern (Fig. S8, SI) of the prepared ZIF-67 matches well with the reported literature [16]. This result demonstrates extra amount of Co^{2+} plays an vital role in formation of the 3D hierarchical flower-like structure. Samples obtained from the comparison experiment 2 also shows that without thermal treatment, no hierarchical structures but the polyhedral ZIF-67 particles are produced (Figs. S7b, S8, SI), indicating thermal treatment is another vital factor that affects formation of the unique structure. In addition, the intermediate product obtained after 0.5 h's solvothermal reaction during time-dependent experiment (Fig. S9, SI) appears in mixture of polyhedral particles and half-blossomed flowers. Accompanying the morphological change from polyhedra to the 3D hierarchical structure composed of 2D ultrathin nanosheets, the composition structure also changes accordingly. The EDX results (Table S1, SI) shows that compared with ZIF-67, the prepared 3DHFLM possesses much less C element and more O species. Also, in comparison with the FTIR spectra of the 3DHFLM illustrated above, the ZIF-67 possesses a completely different spectra (Fig. S4, SI), which shows clear absorption bands ascribed to the entire imidazole ring stretching (1380-1450 cm^{-1}), the in-plane bending (800-1350 cm^{-1}) and the out-of-plane bending (below 800 cm^{-1}) of the ring [50]. However, no such absorption bands associated with the imidazole ring, but the characteristic peaks assigned to aliphatic groups appear in the FTIR spectra of the Co-3DHFLM. Therefore, it can be concluded that the 2-MeIm rings were fractured and the extra Co^{2+} possibly experienced hydrolysis in the solvothermal process.

Based on the above results, the possible formation mechanism of the 3D hierarchical flower-like structure is proposed as follows. When the Co^{2+} and 2-MeIm are mixed in methanol solution, ZIF-67 particles are initially generated in a rapid manner due to strong coordination, which function as intermediate substances for the subsequent transformation and growth. Under the solvothermal condition, the relatively high temperature and pressure in the sealed autoclave supplies a driving force for dissolution of the surface composition of the ZIF particles, which results in fracture of the ordered coordinating system of imidazole ring with Co ions, and the imidazole ring is further fractured to small aliphatic groups. Simultaneously, the extra uncoordinated Co^{2+} functions as predators to capture the dissolved composition, which in turn accelerate the dissolution/fracture process. Co^{2+} ions also undergo a hydrolyzation process in the hot basic environment generated by high concentration of 2-MeIm in methanol forming hydroxide-like compounds. Those compounds simultaneously re-coordinate with the aliphatic groups from destruction of imidazole ring. The produced components crystalize in certain protocol forming nanosheet embryo and grow further constructing the nanosheets cross-linked hierarchical shell. The detailed formation mechanism is still under investigation.

In view of the potential electrochemical properties of the transition-metal based phosphides, we convert the as-prepared precursor 3DHFLMs by treatment with NaH_2PO_2 at a relatively low temperature of 300 °C for 2 h in a nitrogen atmosphere. As shown in the panoramic view of the phosphorized CoNi-3DHFLM (CoNi-P-3DHFLM, Fig. 3), the 3D hierarchical flower-like morphology composed of nanosheets maintain intact after phosphorization without obvious deformation. It is worth noted that the nanosheets are also well-maintained at a very thin level of around 1.6 nm according to the AFM analysis (Fig. S10, SI), which is only slightly thicker than the untreated sample. The TEM images (Fig. 3b) further demonstrate the hierarchical structure is crosslinked by disoriented nanosheets. Furthermore, the TEM image of an enlarged part of a single flower (Fig. 3b2) shows a discontinuous and relatively rough surface with tiny holes, which differs from the continuous and smooth surface of the precursor sample due to the thermal phosphorization process, indicating the phosphorization treatment helps to create in-plane pores on the composing nanosheets, and endows the sample with a high Brunauer-Emmett-Teller (BET) specific surface area of 267.3 $m^2 g^{-1}$ and a large pore size distribution from microporous to mesoporous range (Fig. S11, SI). CoMn-P-3DHFLM and CoCu-P-3DHFLM also experience the same fate as that of CoNi-P-3DHFLM (Figs. S12-13, SI), and the BET specific surface areas of the CoM-3DHFLMs are in the same level (Table S2, SI). Such a unique structure can benefit the electrocatalytic application in the following several aspect: 1) the 3D hierarchical structure composed of the interconnected nanosheets could facilitate the accessibility of electrolyte and accelerate ion diffusion; 2) the ultrathin building blocks and the derived randomly-oriented architecture can help to avert the agglomeration phenomenon usually happened to those catalysts of 0D and 1D structures, and thus supply highly exposed active sites to promote the catalytic activity; and 3) additional active edge sites can be exposed due to the in-plain pores formed upon phosphorization treatment, which render more exposed surface and active sites.

As for the crystal structure, a well resolved crystal lattice fringe spacing of 0.283 nm corresponding to the (001) crystal plane of CoP can be clearly observed from the high resolution TEM image (inset in Fig. 3b2). Fig. 4a shows the CoM-P-3DHFLMs possess a thoroughly different XRD pattern from the precursor CoM-3DHFLMs, which exhibit a higher crystallinity with characteristic diffraction peaks at around 31.7°, 36.4°, 46.4°, 48.3°, 52.3° and 56.6°, corresponding to the (001), (111), (112), (211), (103), and (301) facets of CoP (JCPDS-29-0497), respectively. Also, for the prepared bimetallic CoM-P-3DHFLMs, the same XRD patterns without any other new peaks possibly arising from other metal phosphides or impurities can be observed. These results indicate that the secondary metal homogeneously intercalates into the crystal lattice of CoP and has trivial effect on the lattice constant due to the similar ionic radius of the host and guest metal ions in the crystals [51]. The EDX mapping analysis (Figs. 3c, S12c, 13c, SI) further verifies the homogeneous distribution of the host Co and other guest metal ions in company with P element. The elemental composition status of CoNi-P-3DHFLM were also determined by XPS. Fig. S14 shows the CoNi-P-3DHFLM contains Co, Ni, P, C, N, and O elements. As shown in the high-resolution XPS spectrum of Co 2p (Fig. 4b), the deconvoluted peaks at 793.5 and 778.6 eV can be assigned to the Co 2p1/2 and Co 2p3/2. While the peaks at 797.7 and 781.6 eV are derived from the Co 2p1/2 and Co 2p3/2 of the oxidized Co species, respectively. In addition, other two peaks locating at 786.3 and 803.4 eV are shakeup satellite peak (Sat.) [23,52]. The P species (Fig. 4c) with binding energy of 129.4 and 130.2 eV can be attributed to P bonded to Co and Ni (metal phosphides). The other predominant peak around 134.0 eV derives from PO_4^{3-} [53]. As for Ni (Fig. 4d), the XPS spectrum of Ni 2p3/2 can be deconvoluted into two peaks locating at 853.6 and 856.7, which represent Ni^{2+} and Ni^{3+} species, respectively. While the peaks at 870.8 and 874.7 eV are attributed to Ni 2p 1/2, representing Ni^{3+} species in Ni-P and Ni^{2+} species, respectively. It is worth noting that intercalation of Ni leads to a negative shift in the binding energies of Co 2p3/2 and P 2p3/2 in comparison with the Co-P-3DHFLM, which means the intercalation of the secondary metal ion can cause electronic modulation in the bimetallic 3DHFLMs [17,54]. For Mn and Cu intercalated bimetallic P-3DHFLMs, the XPS spectra also show obvious peaks relating to them (Fig. S15, SI).

The electrocatalytic activity of the prepared samples ((Co, CoNi, CoMn, CoCu)-P-3DHFLMs) toward OER was evaluated using a typical three-electrode system in a 1.0 M KOH solution. According to the linear sweep voltammetry (LSV) curves (Fig. 5a), the CoM-P-3DHFLMs expectedly exhibit more negative potential and higher current density in comparison with the Co-P-3DHFLM, suggesting their better OER performance. The operating potentials required at a current density of 10 mA cm^{-2} (a metric associated with solar fuel synthesis [55]) are also compared (Fig. 5b). In order to achieve a current density of 10 mA cm^{-2}, CoNi/CoMn/CoCu-P-3DHFLMs require overpotentials of 292 mV, 318 mV, and 307 mV, much lower than Co-P-3DHFLM (348 mV) and most of reported noble-metal based and transition-metal-

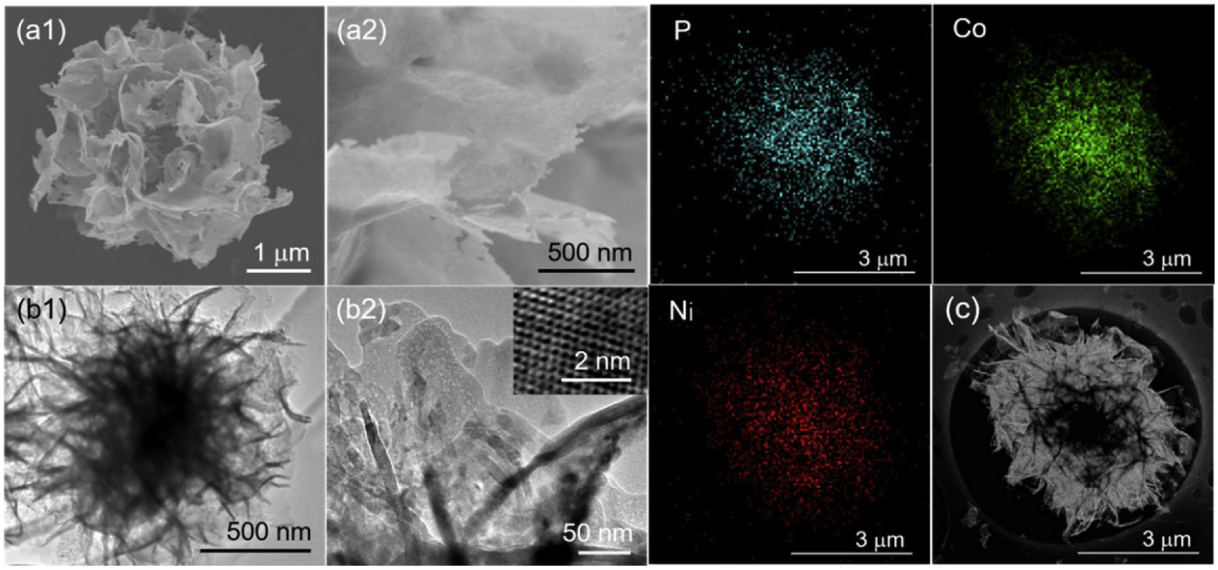

Fig. 3. SEM (a), TEM (b), and HAADF-STEM image with elemental mapping data of the CoNiP-3DHHS (c).

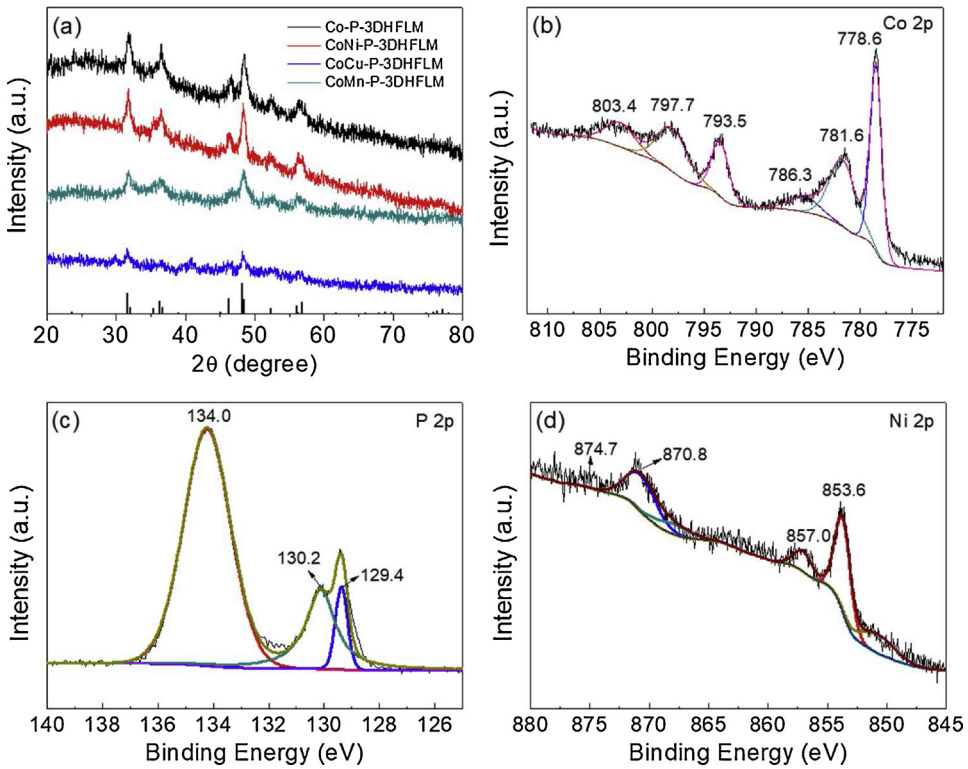

Fig. 4. XRD patterns of the as-prepared phosphorized 3DHFLMs and the peaks' location from the standard JCPDS card No. 29-0497 of CoP (a), high resolution XPS spectra of Co 2p (b), P 2p (c), and Ni 2p in the CoNi-P-3DHFLM.

phosphides catalysts (Table S3, SI). This result is in accordance with other reported bimetallic phosphide materials [16,21,28,56]. Previous studies have demonstrated that the second metal doping can make the d-band center closer to Fermi level and lead to stronger binding interaction between the adsorbates and catalyst, thus essentially contributes to the enhancement of OER activity [57]. It was also reported that homogeneous incorporation of a second metal that is in close proximity to Co atom to CoP species could reduce the oxophilicity of Co, and thus lead to a decrease in the binding energy of the intermediates on Co sites. Therefore, the formed bimetallic phosphide catalyst can effectively modulate the binding energies of the intermediates towards optimal value and thus benefiting OER [17,56]. What is also noteworthy is that although the electrocatalytic activity of Co-P-3DHFLM is ordinary in the prepared 3DHFLMs, it still performs better than the phosphorized CoNi-ZIF particles (P-ZIF), which requires an overpotential of 390 mV to reach a current density of 10 mA cm^{-2} (Fig. S16, SI). This is undoubtedly attributed to the above-described structure privileges derived from the unique 3D hierarchical structures composed of ultrathin nanosheets, which can supply much higher fraction of active sites compared to the bulk nanoparticle counterparts. The Tafel plots derived from the LSV curves of the as-prepared 3DHFLM samples were analyzed to probe their OER kinetics. Fig. 5c shows the Tafel slopes of 84 mV dec^{-1}, 98 mV dec^{-1}, and 88 mV dec^{-1} for CoNi-P-3DHFLM, CoMn-P-3DHFLM, and CoCu-P-3DHFLMs are also higher than that of Co-P-3DHFLM

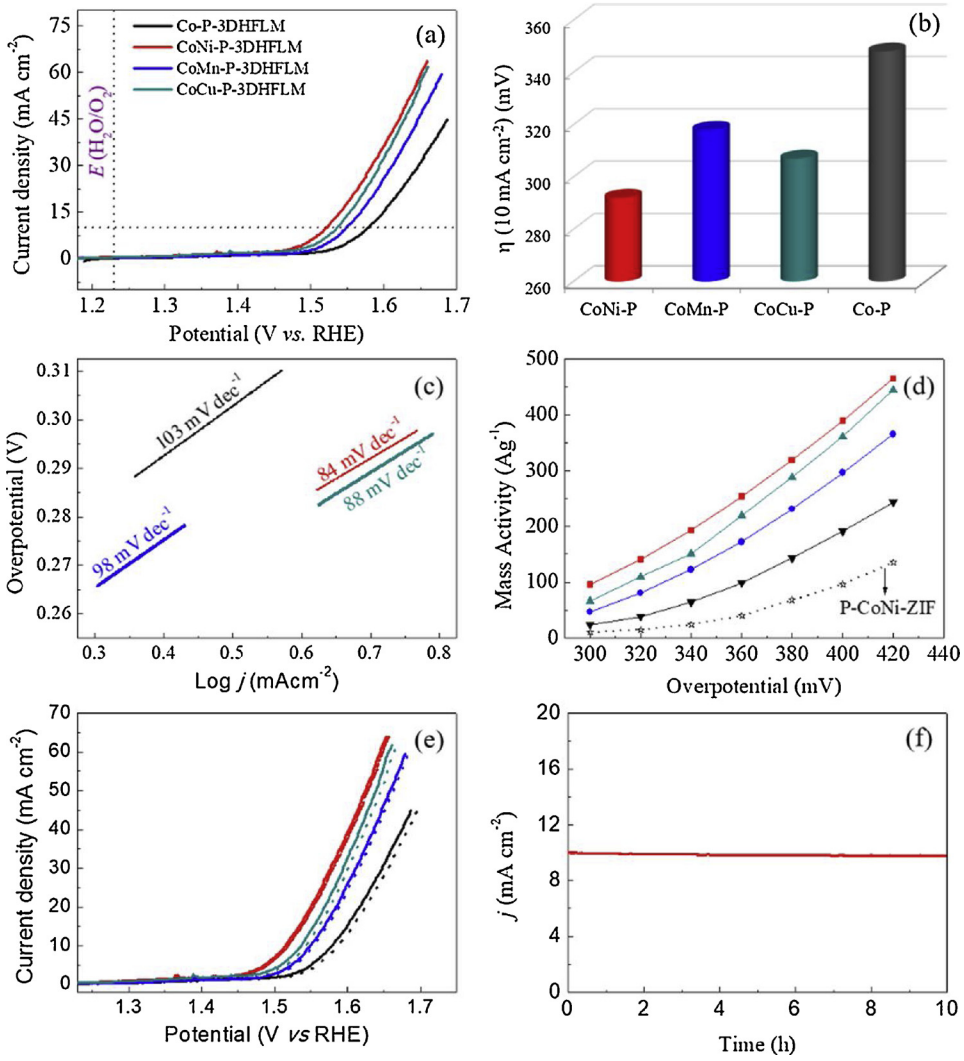

Fig. 5. (a) Polarization curves, (b) Overpotential at the current density of 10 mA cm^{-2}, (c) Tafel plots, (d) Plot of the mass activity versus overpotential, (e) Polarization curves of initially (solid) and after 1500 CV sweeps (dashed), and (f) Chronoamperometry curve of the CoNi-P-3DHFLM measured at 300 mV.

(103 mV dec^{-1}), suggesting the more effective kinetics of bimetallic electrocatalysts in OER. Due to that the real surface area normalized activity (specific activity) has a serious drawback that highly inaccurate data are obtained when normalization is performed using the BET surface area [58], the mass normalized activity (mass activity) that is currently gaining importance in evaluation of nanostructured electrocatalysts for OER was performed to looking further into the OER activity of the prepared products. The calculated mass activity values were plotted against their respective overpotentials. Fig. 5d shows the mass activity of the prepared catalysts calculated in the overpotential range from 300 to 420 mV (1.53 to 1.65 V vs RHE) at an interval of 20 mV. It can be witnessed that with the same mass loading of 0.127 mg cm^{-2}, the prepared 3DHFLMs show better OER activity than the P-ZIF particles. At a designated overpotential of 360 mV, the calculated mass activities of the prepared samples are 253, 172, 219 and 98 A g^{-1} for CoNi-, CoMn-, CoCu- and Co-3DHFLMs, respectively. In comparison, the P-ZIF exhibits a much lower mass activity of 40 A g^{-1}. Such a mass activity trend not only advocates the superior OER activity of the 3DHFLMs with unique structures, but also proves the advantages of bimetallic improvement. Notably, due to the structure and composition privileges, the prepared CoM-P-3DHFLMs can achieve comparable even higher catalytic activity than other reported phosphide catalysts with less catalyst loading (Table S3, SI).

To unveil the underlying mechanism of the improved OER performance, the electrochemical double-layer capacitance (C_{dl}), which is proportional to electrochemical active surface area (ECSA) [59], was also evaluated. To evaluate the ECSA, C_{dl} was calculated by monitoring the cyclic voltammetry (CV) curves in the potential range of 1.4–1.5 V without redox processes at increasing scan rates. As shown in Fig. S17, C_{dl} of the CoM-P-3DHFLMs (145.0 m F cm^{-2}, 103.3 m F cm^{-2}, and 140.9 m F cm^{-2} for CoNi-P-3DHFLM, CoMn-P-3DHFLM, and CoCu-P-3DHFLM, respectively) are much larger than that of CoP (77.3 m F cm^{-2}). The larger electrochemical double-layer capacitance indicates that CoM-P-3DHFLMs expose higher active sites, which may be one of the possible reasons for improved OER performance. Considering that the charge transfer resistance strongly affects the electrocatalytic activities of catalysts, enhancement of charge transfer can boost the combination of reactants and electrocatalysts and promotes the electrocatalytic activity. Therefore, electrochemical impedance spectroscopy (EIS) of the prepared 3DHFLMs was also performed to further study the electrode reaction kinetics. As evidenced by the Nyquist plots (Fig. S18, SI) of the catalysts, the charge transfer resistances (R_{ct}) of the prepared 3DHFLMs are in the trend of Co-P > CoMn-P > CoNi-P > CoCu-P, indicating the charge transfer rates of CoM-P-3DHFLMs are faster, and thus results in the enhancement of the electrocatalytic activities for OER.

As a catalyst, stability is also a vital criterion to evaluate its applicability. For this purpose, chronoamperometry and continuous cyclic

voltammetry (CV) tests of the 3DHFLMs were conducted to assess the long-term stability. As shown in Fig. 5e, the LSV of all the samples after 1500 cycles exhibit negligible change in comparison with the initial one. The CV curves of the representative CoNi-P-3DHFLM also shows the same phenomenon (Fig. S19, SI). The Chronoamperometry curve of the CoNi-P-3DHFLM and other three tested samples (Figs. 5f and S20, SI) shows a relatively stable current density over 15 h. These results prove the as-prepared 3DHFLMs keep high stability during the long-term OER processes. To penetrate further into the stability of the catalysts, we carried out the post surface composition analysis on both morphological and elemental structures. Fig. S21 shows that after 15 h' OER reaction, the morphological structure of the CoNi-P-3DHFLM maintained well with no obvious change from the unused sample. While, it can be found from the EDX analysis (Table S4, SI) that elemental composition experienced a small change reflecting mainly on increase of the O element. This result is not out of expectation. Many previous studies have shown that metal phosphides (i.e. CoP, Ni_2P) possess high sensitivity to air and are prone to partial oxidation [17,60]. However, it has also been proved that the in-situ electrochemically formed oxidized layer on the original composition layer is more energetically favorable for OER activity [41], which means that the partially oxidized species behaves not an obstacle but a propeller. Therefore, the well-maintained hierarchically flower-like structure and the favorable composition concomitantly contribute to the long-term stability of the catalyst.

3. Conclusions

In summary, we report here a facile one-pot bottom-up solvothermal strategy for synthesizing Cobalt based bimetallic phosphides of 3D hierarchical flower-like superstructure composed of 2D ultrathin nanosheets as electrocatalysts for oxygen evolution reaction, which shows highly efficient and durable electrocatalytic activity because of the structural and compositional features. Specifically, CoNi, CoMn, and CoCu-P-3DHFLMs require only 292 mV, 318 mV, and 307 mV, respectively to achieve the current density of 10 mA cm^{-2}, which are comparable and even better than the commercially available noble-metal based catalysts. This work offers a promising candidate for OER with the privileges of high efficiency, long-term stability and cost-effectiveness.

Acknowledgements

This work was jointly supported by the funding support from the National Natural Science Foundation of China (No. 21876192, 21677159, 21677167, and 21522706), the National Key Research Development Program of China (2016YFA0203102), and the Thousand Young Talents Program of China.

Appendix A. Supplementary data

Supplementary material related to this article can be found, in the online version, at doi:https://doi.org/10.1016/j.apcatb.2019.03.007.

References

[1] H. Li, Y. Sun, Z.-Y. Yuan, Y.-P. Zhu, T.-Y. Ma, Titanium phosphonate based metal-organic frameworks with hierarchical porosity for enhanced photocatalytic hydrogen evolution, Angew. Chem. Int. Ed. 57 (2018) 3222–3227.
[2] W. Liu, J. Huang, Q. Yang, S. Wang, X. Sun, W. Zhang, J. Liu, F. Huo, Multi-shelled hollow metal-organic frameworks, Angew. Chem. Int. Ed. 56 (2017) 5512–5516.
[3] L. Huang, R. Chen, C. Xie, C. Chen, Y. Wang, Y. Zeng, D. Chen, S. Wang, Rapid cationic defect and anion dual-regulated layered double hydroxides for efficient water oxidation, Nanoscale 10 (2018) 13638–13644.
[4] Y. Wang, D. Yan, S. El Hankari, Y. Zou, S. Wang, Recent progress on layered double hydroxides and their derivatives for electrocatalytic water splitting, Adv. Sci. 5 (2018) 1800064.
[5] S. Cai, Z. Meng, H. Tang, Y. Wang, P. Tsiakaras, 3D Co-N-doped hollow carbon spheres as excellent bifunctional electrocatalysts for oxygen reduction reaction and oxygen evolution reaction, Appl. Catal. B-Environ. 217 (2017) 477–484.
[6] G.-R. Zhang, S. Woellner, Hollowed structured PtNi bifunctional electrocatalyst with record low total overpotential for oxygen reduction and oxygen evolution reactions, Appl. Catal. B-Environ. 222 (2018) 26–34.
[7] C.L. Tan, H. Zhang, Two-dimensional transition metal dichalcogenide nanosheet-based composites, Chem. Soc. Rev. 44 (2015) 2713–2731.
[8] Z. Huang, A. Zhou, J. Wu, Y. Chen, X. Lan, H. Bai, L. Li, Bottom-up preparation of ultrathin 2D aluminum oxide nanosheets by duplicating graphene oxide, Adv. Mater. 28 (2016) 1703–1708.
[9] J. Xie, H. Zhang, S. Li, R. Wang, X. Sun, M. Zhou, J. Zhou, X.W. Lou, Y. Xie, Defect-rich MoS_2 ultrathin nanosheets with additional active edge sites for enhanced electrocatalytic hydrogen evolution, Adv. Mater. 25 (2013) 5807–5813.
[10] X. Huang, Z.Y. Zeng, H. Zhang, Metal dichalcogenide nanosheets: preparation, properties and applications, Chem. Soc. Rev. 42 (2013) 1934–1946.
[11] L.K. Li, Y.J. Yu, G.J. Ye, Q.Q. Ge, X.D. Ou, H. Wu, D.L. Feng, X.H. Chen, Y.B. Zhang, Black phosphorus field-effect transistors, Nat. Nanotechnol. 9 (2014) 372–377.
[12] Y. Zeng, Y. Wang, G. Huang, C. Chen, L. Huang, R. Chen, S. Wang, Porous CoP nanosheets converted from layered double hydroxides with superior electrochemical activity for hydrogen evolution reactions at wide pH ranges, Chem. Commun. 54 (2018) 1465–1468.
[13] M. Zhao, Y. Huang, Y. Peng, Z. Huang, Q. Ma, H. Zhang, Two-dimensional metal-organic framework nanosheets: synthesis and applications, Chem. Soc. Rev. 47 (2018) 6267–6295.
[14] H. Yan, C. Tian, L. Wang, A. Wu, M. Meng, L. Zhao, H. Fu, Phosphorus-modified tungsten nitride/reduced graphene oxide as a high-performance, non-noble-metal electrocatalyst for the hydrogen evolution reaction, Angew. Chem. Int. Ed. 54 (2015) 6325–6329.
[15] H.F. Ye, R. Shi, X. Yang, W.F. Fu, Y. Chen, P-doped ZnxCd1-xS solid solutions as photocatalysts for hydrogen evolution from water splitting coupled with photocatalytic oxidation of 5-hydroxymethylfurfural, Appl. Catal. B-Environ. 233 (2018) 70–79.
[16] P. He, X.-Y. Yu, X.W. Lou, Carbon-incorporated nickel-cobalt mixed metal phosphide nanoboxes with enhanced electrocatalytic activity for oxygen evolution, Angew. Chem. Int. Ed. 56 (2017) 3897–3900.
[17] X. Xiao, C.-T. He, S. Zhao, J. Li, W. Lin, Z. Yuan, Q. Zhang, S. Wang, L. Dai, D. Yu, A general approach to cobalt-based homobimetallic phosphide ultrathin nanosheets for highly efficient oxygen evolution in alkaline media, Energy Environ. Sci. 10 (2017) 893–899.
[18] D.-H. Ha, B. Han, M. Risch, L. Giordano, K.P.C. Yao, P. Karayaylali, Y. Shao-Horn, Activity and stability of cobalt phosphides for hydrogen evolution upon water splitting, Nano Energy 29 (2016) 37–45.
[19] Z.-H. Xue, H. Su, Q.-Y. Yu, B. Zhang, H.-H. Wang, X.-H. Li, J.-S. Chen, Janus Co/CoP nanoparticles as efficient Mott-Schottky electrocatalysts for overall water splitting in wide pH range, Adv. Energy Mater. 7 (2017) 1602355.
[20] S. Kampouri, T.N. Nguyen, C.P. Ireland, B. Valizadeh, F.M. Ebrahim, G. Capano, D. Ongari, A. Mace, N. Guijarro, K. Sivula, A. Sienkiewicz, L. Forro, B. Smit, K.C. Stylianou, Photocatalytic hydrogen generation from a visible-light responsive metal-organic framework system: the impact of nickel phosphide nanoparticles, J. Mater. Chem. A Mater. Energy Sustain. 6 (2018) 2476–2481.
[21] E. Hu, Y. Feng, J. Nai, D. Zhao, Y. Hu, X.W. Lou, Construction of hierarchical Ni-Co-P hollow nanobricks with oriented nanosheets for efficient overall water splitting, Energy Environ. Sci. 11 (2018) 872–880.
[22] T. Wang, C. Wang, Y. Jin, A. Sviripa, J. Liang, J. Han, Y. Huang, Q. Li, G. Wu, Amorphous Co-Fe-P nanospheres for efficient water oxidation, J. Mater. Chem. A 5 (2017) 25378–25384.
[23] B. Qiu, L. Cai, Y. Wang, Z. Lin, Y. Zuo, M. Wang, Y. Chai, Fabrication of nickel-cobalt bimetal phosphide nanocages for enhanced oxygen evolution catalysis, Adv. Funct. Mater. 28 (2018) 1706008.
[24] X.-Y. Yu, Y. Feng, B. Guan, X.W. Lou, U. Paik, Carbon coated porous nickel phosphides nanoplates for highly efficient oxygen evolution reaction, Energy Environ. Sci. 9 (2016) 1246–1250.
[25] K.W. Tseng, S.B. Huang, W.C. Chang, H.Y. Tuan, Synthesis of mesoporous germanium phosphide microspheres for high-performance lithium-ion and sodium-ion battery anodes, Chem. Mater. 30 (2018) 4440–4447.
[26] Y. Kim, Y. Kim, A. Choi, S. Woo, D. Mok, N.S. Choi, Y.S. Jung, J.H. Ryu, S.M. Oh, K.T. Lee, Tin phosphide as a promising anode material for Na-ion batteries, Adv. Mater. 26 (2014) 4139–4144.
[27] D.-S. Yang, D. Bhattacharjya, S. Inamdar, J. Park, J.-S. Yu, Phosphorus-doped ordered mesoporous carbons with different lengths as efficient metal-free electrocatalysts for oxygen reduction reaction in alkaline media, J. Am. Chem. Soc. 134 (2012) 16127–16130.
[28] B.Y. Guan, L. Yu, X.W. Lou, General synthesis of multishell mixed-metal oxyphosphide particles with enhanced electrocatalytic activity in the oxygen evolution reaction, Angew. Chem. Int. Ed. 56 (2017) 2386–2389.
[29] J. Chang, Y. Xiao, M. Xiao, J. Ge, C. Liu, W. Xing, Surface oxidized cobalt-phosphide nanorods as an advanced oxygen evolution catalyst in alkaline solution, ACS Catal. 5 (2015) 6874–6878.
[30] D.A. Reddy, H.K. Kim, Y. Kim, S. Lee, J. Choi, M.J. Islam, D.P. Kumar, T.K. Kim, Multicomponent transition metal phosphides derived from layered double hydroxide double-shelled nanocages as an efficient non-precious cocatalyst for hydrogen production, J. Mater. Chem. A 4 (2016) 13890–13898.
[31] H. Furukawa, K.E. Cordova, M. O'Keeffe, O.M. Yaghi, The chemistry and applications of metal-organic frameworks, Science 341 (2013) 974–986.
[32] S. Wang, C.M. McGuirk, A. d'Aquino, J.A. Mason, C.A. Mirkin, Metal-organic framework nanoparticles, Adv. mater. 30 (2018) 1800202.

[33] H. Zhao, Y. Chen, Q. Peng, Q. Wang, G. Zhao, Catalytic activity of MOF(2Fe/Co)/carbon aerogel for improving H_2O_2 and (OH)-O-center dot generation in solar photo-electro-Fenton process, Appl. Catal. B-Environ. 203 (2017) 127–137.
[34] W. Zhu, C. Zhang, Q. Li, L. Xiong, R. Chen, X. Wan, Z. Wang, W. Chen, Z. Deng, Y. Peng, Selective reduction of CO_2 by conductive MOF nanosheets as an efficient co-catalyst under visible light illumination, Appl. Catal. B-Environ. 238 (2018) 339–345.
[35] H.B. Wu, X.W. Lou, Metal-organic frameworks and their derived materials for electrochemical energy storage and conversion: promises and challenges, Sci. Adv. 3 (2017) 9252.
[36] X.-F. Lu, L.-F. Gu, J.-W. Wang, J.-X. Wu, P.-Q. Liao, G.-R. Li, Bimetal-organic framework derived $CoFe_2O_4$/C porous hybrid nanorod arrays as high-performance electrocatalysts for oxygen evolution reaction, Adv. Mater. 29 (2017) 1604437.
[37] J.A. Vigil, T.N. Lambert, B.T. Christensen, Cobalt phosphide-based nanoparticles as bifunctional electrocatalysts for alkaline water splitting, J. Mater. Chem. A 4 (2016) 7549–7554.
[38] S.T. Meek, J.A. Greathouse, M.D. Allendorf, Metal-organic frameworks: a rapidly growing class of versatile nanoporous materials, Adv. Mater. 23 (2011) 249–267.
[39] J. Lee, J.H. Kwak, W. Choe, Evolution of form in metal-organic frameworks, Nat. Commun. 8 (2017) 14070.
[40] X.-Y. Liu, F. Zhang, T.-W. Goh, Y. Li, Y.-C. Shao, L. Luo, W. Huang, Y.-T. Long, L.-Y. Chou, C.-K. Tsung, Using a multi-shelled hollow metal-organic framework as a host to switch the guest-to-host and guest-to-guest interactions, Angew. Chem. Int. Ed. 57 (2018) 2110–2114.
[41] Z. Liu, Y. Wang, R. Chen, C. Chen, H. Yang, J. Ma, Y. Li, S. Wang, Quaternary bimetallic phosphosulphide nanosheets derived from prussian blue analogues: origin of the ultra-high activity for oxygen evolution, J. Power Sources 403 (2018) 90–96.
[42] R.S. McEwen, Crystallographic studies on nickel hydroxide and higher nickel oxides, J. Phys. Chem. 75 (1971) 1782–1789.
[43] M. Dixit, G.N. Subbanna, P.V. Kamath, Homogeneous precipitation from solution by urea hydrolysis: a novel chemical route to the alpha-hydroxides of nickel and cobalt, J. Mater. Chem. 6 (1996) 1429–1432.
[44] Y.C. Zhu, H.L. Li, Y. Koltypin, A. Gedanken, Preparation of nanosized cobalt hydroxides and oxyhydroxide assisted by sonication, J. Mater. Chem. 12 (2002) 729–733.
[45] J. Zhang, Q. Kong, L. Yang, D.-Y. Wang, Few layered $Co(OH)_2$ ultrathin nanosheet-based polyurethane nanocomposites with reduced fire hazard: from eco-friendly flame retardance to sustainable recycling, Green Chem. 18 (2016) 3066–3074.
[46] M. Aghazadeh, H.M. Shiri, A.-A.M. Barmi, Uniform beta-$Co(OH)_2$ disc-like nanostructures prepared by low-temperature electrochemical rout as an electrode material for supercapacitors, Appl. Surf. Sci. 273 (2013) 237–242.
[47] Z.-A. Hu, Y.-L. Xie, Y.-X. Wang, L.-J. Xie, G.-R. Fu, X.-Q. Jin, Z.-Y. Zhang, Y.-Y. Yang, H.-Y. Wu, Synthesis of alpha-cobalt hydroxides with different intercalated anions and effects of intercalated anions on their morphology, basal plane spacing, and capacitive property, J. Phys. Chem. C 113 (2009) 12502–12508.
[48] H.T. Sun, X. Sun, T. Hu, M.P. Yu, F.Y. Lu, J. Lian, Graphene-wrapped mesoporous cobalt oxide hollow spheres anode for high-rate and long-life lithium ion batteries, J. Phys. Chem. C 118 (2014) 2263–2272.
[49] E. Desimoni, B. Brunetti, X-ray photoelectron spectroscopic characterization of chemically modified electrodes used as chemical sensors and biosensors: a review, Chemosensors 3 (2015) 70–117.
[50] S. Dou, C.-L. Dong, Z. Hu, Y.-C. Huang, J.-L. Chen, L. Tao, D. Yan, D. Chen, S. Shen, S. Chou, S. Wang, Atomic-scale CoOx species in metal-organic frameworks for oxygen evolution reaction, Adv. Funct. Mater. 27 (2017) 1702546.
[51] Z.-F. Huang, J. Song, K. Li, M. Tahir, Y.-T. Wang, L. Pan, L. Wang, X. Zhang, J.-J. Zou, Hollow cobalt-based bimetallic sulfide polyhedra for efficient all-pH-value electrochemical and photocatalytic hydrogen evolution, J. Am. Chem. Soc. 138 (2016) 1359–1365.
[52] C. Xia, Q. Jiang, C. Zhao, M.N. Hedhili, H.N. Alshareef, Selenide-based electrocatalysts and scaffolds for water oxidation applications, Adv. Mater. 28 (2016) 77–85.
[53] R.Q. Ye, P. del Angel-Vicente, Y.Y. Liu, M.J. Arellano-Jimenez, Z.W. Peng, T. Wang, Y.L. Li, B.I. Yakobson, S.H. Wei, M.J. Yacaman, J.M. Tour, High-performance hydrogen evolution from MoS2(1-x)P (x) solid solution, Adv. Mater. 28 (2016) 1427–1432.
[54] Y. Tan, H. Wang, P. Liu, Y. Shen, C. Cheng, A. Hirata, T. Fujita, Z. Tang, M. Chen, Versatile nanoporous bimetallic phosphides towards electrochemical water splitting, Energy Environ. Sci. 9 (2016) 2257–2261.
[55] T.Y. Ma, S. Dai, M. Jaroniec, S.Z. Qiao, Metal-organic framework derived hybrid Co_3O_4-carbon porous nanowire arrays as reversible oxygen evolution electrodes, J. Am. Chem. Soc. 136 (2014) 13925–13931.
[56] X. Feng, X. Bo, L. Guo, CoM(M = Fe,Cu,Ni)-embedded nitrogen-enriched porous carbon framework for efficient oxygen and hydrogen evolution reactions, J. Power Sources 389 (2018) 249–259.
[57] X.-L. Wang, L.-Z. Dong, M. Qiao, Y.-J. Tang, J. Liu, Y. Li, S.-L. Li, J.-X. Su, Y.-Q. Lan, Exploring the performance improvement of the oxygen evolution reaction in a stable bimetal-organic framework system, Angew. Chem. Int. Ed. 57 (2018) 9660–9664.
[58] S. Anantharaj, S.R. Ede, K. Karthick, S.S. Sankar, K. Sangeetha, P.E. Karthik, S. Kundu, Precision and correctness in the evaluation of electrocatalytic water splitting: revisiting activity parameters with a critical assessment, Energy Environ. Sci. 11 (2018) 744–771.
[59] H.B. Wu, B.Y. Xia, L. Yu, X.-Y. Yu, X.W. Lou, Porous molybdenum carbide nano-octahedrons synthesized via confined carburization in metal-organic frameworks for efficient hydrogen production, Nat. Commun. 6 (2015) 6512.
[60] Y. Zhang, B. Ouyang, J. Xu, G. Jia, S. Chen, R.S. Rawat, H.J. Fan, Rapid synthesis of cobalt nitride nanowires: highly efficient and low-cost catalysts for oxygen evolution, Angew. Chem. Int. Ed. 55 (2016) 8670–8674.